J Mater Sci (2018) 53:8020–8029

Biomaterials

Catalytic conversion of Kraft lignin to bio-multilayer graphene materials under different atmospheres

Qiangu Yan[1], Xuefeng Zhang[1], Jinghao Li[2,3,*], El Barbary Hassan[1], Chuji Wang[4], Jilei Zhang[1,*], and Zhiyong Cai[3,*]

[1] Department of Sustainable Bioproducts, Mississippi State University, Mississippi State, MS 39762, USA
[2] Department of Biomaterials, International Center for Bamboo and Rattan, Beijing 10000, China
[3] Forest Products Lab, USDA Forest Service, Madison, WI 53726, USA
[4] Department of Physics and Astronomy, Mississippi State University, Mississippi State, MS 39762, USA

Received: 11 January 2018
Accepted: 23 February 2018
Published online: 5 March 2018

ABSTRACT

Kraft lignin was catalytic graphitized by iron at 1000 °C in argon, hydrogen, CO_2, methane, and natural gas atmospheres, respectively. The effect of atmospheric agent types on product distribution (gas, liquid, and solid carbon yields) was analyzed. The solid products were characterized by scanning electron microscopy, Raman, high-resolution transmission electron microscopy, and X-ray diffraction. Experimental results have shown that the degree of graphitization of Kraft lignin depends not only on the highest temperature, but also the type of ambient gas phase during heat treatment. Methane and natural gas in the ambient gas phase seem to accelerate the formation of multilayer graphene materials with a range of 2–30 layers, and hydrogen and carbon dioxide have an etching effect on solid carbon species during the catalytic graphitization process, while multilayer graphene-encapsulated iron nanoparticles were the main products in the case of argon.

Introduction

It has been reported that the graphitization of solid carbon-based species is mainly affected by the heat treatment temperature [1], while other heat treatment variables like residence time and heating rate have a slight effect on the degree of graphitization of the products [2]. It was claimed that ambient gas phase had a relatively large effect on graphitization of solid carbon [3]. A purging gas is usually used to remove the volatiles released from carbonaceous materials and generate a protective or a reactive atmosphere during the carbonization/graphitization processes [4]. There are two types of gases used in the carbonization/graphitization process: inert gas [5] and reactive gases [6]. Typically, inert gases like nitrogen, argon, and helium are used as the purging gas during the carbonization/graphitization processes. However, the carbonization/graphitization process has also been carried out with reactive gases like CO_2, steam (H_2O), or hydrogen. The reactive gases can be

Address correspondence to E-mail: jli@fs.fed.us; jz27@msstate.edu; zcai@fs.fed.us

https://doi.org/10.1007/s10853-018-2172-0

classified to two categories: (i) reducing gases, i.e., H_2 and hydrocarbons [7–9], and (ii) oxidizing gases: CO_2, steam, O_2, and air [2, 3, 6]. Graphitization efficiency and graphitization temperature were reportedly affected by residual elements such as hydrogen, nitrogen, oxygen, and chlorine [6]. The presence of gaseous oxidizer, e.g., oxygen, carbon dioxide, and water vapor, can enhance graphitization of solid carbon resources [2]. Noda and Inagaki [2, 3] investigated the effect of gas phase on graphitization of a petroleum coke and a carbon black. The experimental results showed that the degree of graphitization of carbon was significantly affected by the ambient gas phase during heat treatment. The presence of oxygen in the ambient gas phase accelerates graphitization, and carbon dioxide had a similar but lesser effect, while no noticeable influence was detected in the cases of nitrogen and argon. Oxygen-containing gases were reported to affect the CNT structures [10–13]. The formation of amorphous carbon was retarded by the presence of mild gaseous oxidizers (e.g., CO_2 and H_2O) [6, 8, 14]. Although nitrogen is usually regarded as an inert gas under low temperature, it is active at high temperature. Nomura et al. [15] investigated the graphitization of solid carbon with uranium carbide (UC) under nitrogen atmosphere. Results showed that the degree of graphitization increased with increasing temperature and increased with decreasing nitrogen pressure. The dependence of graphitization on nitrogen pressure was well explained by a thermodynamic reaction analysis of UC with nitrogen gas. Hydrogen has been widely used for production of carbon nanotubes (CNTs) and graphene in chemical vapor deposition (CVD) process; it plays a very important role in activation of surface-bound carbon and gasification of disordered carbon that will inhibit the graphene growth. Graphene could not be grown without the aid of H_2 in CVD process [9]. However, the presence of H_2 in CVD was reported to degrade the crystallinity of graphene and slows down the growth rate on the Cu catalyst [16] since hydrogen is competing with hydrocarbons on surface active sites of the catalyst, which inhibits growth of graphene [17]. H_2 has strong etching effect on graphene or other ordered carbon species in the presence of transition metals, which destroys the ability of graphene to form hydrocarbons [18]. Light hydrocarbons (e.g., methane, ethane, and propane) are the most common carbon precursors for the growth of ordered carbon forms like CNTs and graphene [19–21].

Previous experimental results indicated graphene formation from lignin both via CVD and thermal annealing solid carbon [22–25]. Graphene growth from CVD process requires low activation energy and tends to form large size graphene sheets. Thermal annealing solid carbon-derived graphene has relative small size and requires high activation energy. CVD graphene growth requires carbon-containing gaseous precursors. About 50–60% carbon in lignin is released as carbonaceous gases, and the rest is left as solid. Therefore, a probable way to increase the yield and selectivity of graphene materials is to gasify the solid carbon residue of Kraft lignin. Hydrogen and carbon dioxide have an etching effect on amorphous carbon [26, 27].

Different types of processing atmospheres will be used to investigate the production of graphene materials from Kraft lignin. Gases will be selected from CH_4, H_2, CO_2, and their mixture to examine effects of processing atmospheres on product component distributions. The object of current work is to investigate catalytic conversion of Kraft lignin to graphene nanomaterials in an inert gas—argon, and reactive gases—hydrogen, methane, natural gas, and CO_2 atmospheres. Special attention is paid to the nanomaterial formation from Kraft lignin under different gases (H_2, CO, CO_2, and CH_4) through a catalytic graphitization process.

Experiments

Materials

Kraft lignin (KL) was provided by Domtar (North Caroline, US), and dried in an oven at 105 °C for 5 h. The content of C, H, and O was 65.89, 7.49, and 26.32%, while proximate analysis showed the content of volatile, fixed carbon, and ash as 54.49, 43.11, and 2.40%.

The promotion of iron ions on the Kraft lignin

The Kraft lignin with iron ions was prepared by the co-precipitation method. Three hundred grams of Kraft lignin was first added to 300 mL tetrahydrofuran in a 2000-mL glass beaker and stirred for 2 h;

246.0 grams of iron(III) nitrate nonahydrate was added to 100 mL DI water in a 500-mL glass beaker, stirred until dissolved completely, followed by adding the iron nitrate solution drop-like to Kraft lignin solution and stirred for 2 h. The mixture was kept at room temperature for 24 h and then transferred to an oven where it was dried at 110 °C for 24 h.

Thermal treatment under different atmospheres

Different process gases—argon, hydrogen (H_2), methane (CH_4), carbon dioxide (CO_2), and natural gas (NG)—were compared in graphene nanomaterial production from Kraft lignin. Fifteen grams of the iron-promoted Kraft lignin was packed in the middle of a 1-inch OD, stainless steel tubular reactor. The process gas was introduced into the reactor at a flow rate of 80 mL/min. The reactor was heated, temperature-programmed with a rate of 10 °C/min to 1000 °C and kept at 1000 °C for 1 h. The furnace was cooled down by 10 °C/min to room temperature.

Characterization

X-ray powder diffraction (XRD) patterns of the samples were obtained using a Rigaku ultima III X-ray diffraction system operated at 40 kV and 44 mA using Cu-Kα radiation with a wavelength of 1.5406 Å, from 20° to 80° at a scan rate of 0 02°s − 1. The morphology of the samples was investigated with a scanning electron microscope (SEM). The sample particle sizes were examined with a JEOL JEM-100CX II transmission electron microscope (TEM) operated at accelerating voltage of 200 kV. Raman spectroscopy measurements were carried out on a Jobin–Yvon microspectrometer equipped with an excitation laser source emitting at 514 nm and an incident power around 1 mW on a thin surface. Twenty spectra were collected for each sample. The crystalline size along the a-axis (La) was calculated using the Cançado equation [28]. Surface area of the solid samples has been determined by N_2 adsorption–desorption (Quantachrome, Autosorb-1). Prior to measurements, the samples were degassed at 300 °C for 3 h.

Results and discussion

Effect of atmosphere on catalytic decomposition of Fe-lignin

The purpose of purging gas use is to remove volatiles from the reaction environment during the biomass conversion process. Previous works have been done in conversion (gasification or pyrolysis or combustion or liquefaction) of solid carbon resources (biomass or coals or chars) under different atmospheres [29]. Usually, inert gases like nitrogen are used as the carrier gas. However, the pyrolysis process has also been carried out with CO_2, steam, or hydrogen as the purge gas [30]. Some previous efforts [4] have demonstrated that the type of carrier gas employed affects both the char yield and properties. The presence of H_2 during pyrolysis significantly increases the yield of tar and the fluidity of coal. Therefore, use of hydrogen as the carrier gas may change a char's morphology significantly due to the strong association between char structure and thermoplastic properties and evolution of volatile matter [4]. In this study, argon, hydrogen, carbon dioxide, methane, and natural gas (NG) were used to compare effects of purging gas on the catalytic thermal decomposition of Kraft lignin. Table 1 lists the product yields of Fe-lignin decomposition in the fixed bed reactor. The result showed that the thermal decomposition of Fe-lignin under argon atmosphere gave a solid carbon yield of 31.3 wt%; the solid carbon yields under CH_4 and natural gas were 36.5 and 36%, respectively, which were the highest compared to 14.7 and 28.8% obtained under CO_2 and H_2 atmospheres, respectively. This can be explained by the fact that more lignin components are converted into gases or liquid products with reactive atmospheres (see supplement Table 1). Thermal treatment under the reducing gas flow makes these condensable species crack over nanosized iron particles. Thermal decomposition of Fe-lignin under H_2 atmosphere produced 19% liquid products (mainly water), the highest compared to 18, 13.5, 13.2, and 10.1% under Ar, natural gas, methane, and CO_2 atmospheres, respectively. This is probably related to the conversion of oxygen in oil fraction which is catalytically converted to water under H_2 atmosphere. Table 1 demonstrates that decomposition of Fe-lignin under CO_2 atmosphere gave gaseous phase yield of 75.2%, the highest compared to 52.2, 50.7, 50.5, and 50.2% under H_2, Ar, natural gas, and

CH_4 atmospheres, respectively. Thermal decomposition of Fe-lignin under CO_2 atmosphere produced the least solid carbon and liquid products and more gaseous products than other atmospheres. This result can be attributed to lignin and its char being gasified by CO_2 at high temperature, and can be further proved by exhibiting the highest CO yield under CO_2 atmosphere.

Characterization of solid residue

X-ray diffraction (XRD) analyses

Figure 1 shows the XRD patterns of solid residues of the 10% Fe-lignin thermal-treated at 1000°C under different atmospheres. The type of atmosphere, the presence of alloying elements (carbon), and the heat treatment temperature influenced the phase composition and microstructure of the formed solid residues of the Fe-lignin samples.

Figure 1a shows the XRD pattern of the Fe-Lignin sample under an argon flow at 1000°C. The diffraction peaks contributed by α-Fe (at 44.6°, 65.0°, and 82.3°) and γ-Fe (at 43.6°, 51.0°, and 75.1°) phases were observed. Three peaks at 43.50°, 50.64°, and 74.36° that corresponded to the γ-iron (1 1 1), (2 0 0) and (2 2 0) planes. The peaks 37.75°, 40.7°, 42.6°, 43.75°, 44.56°, 44.94°, 45.86°, 49.12°, and 57.8° were assigned to cementite, Fe_3C with correspondence planes of (1 2 1), (2 1 0), (2 0 1), (2 1 1), (1 0 2), (2 2 0), (0 3 1), (1 1 2), and (2 2 1), respectively.

The pattern of the Fe-lignin sample thermal-treated with hydrogen had peaks at about 43.6°, 51.0°, and 75.1° (Fig. 1b), all of which were characteristic peaks of γ-iron (austenite). The Fe-lignin sample thermal-treated under hydrogen also had peaks at about 44.5° and 65°, both of which corresponded to α-Fe (Fig. 1b). The difference between the samples from argon and hydrogen was that no Fe_3C peaks were detected for the sample produced under H_2 atmosphere. Hydrogen is well known for its deleterious effect on the mechanical properties of metals and alloys. With the existence of H_2, Fe_3C is decarburized by hydrogen through the methane formation reaction ($Fe_3C + 2H_2 \rightarrow 3Fe + CH_4$.) [24]: The activity of carbon in Fe_3C was reported to be much higher than that in iron phases, as hydrogen reacts more rapidly with carbon in Fe_3C than when dissolved in γ-Fe. Therefore, with the existence of hydrogen, the decarburization rate is greater in the case of cementite than that of α-Fe and γ-Fe. Carbon in alloys with iron is more stable with hydrogen than is cementite, which is an endothermic compound. Hydrogen reacts with cementite and carbon through the following reactions:

$$Fe_3C + 2H_2 \rightarrow 3Fe + CH_4,$$

$$C + 2H_2 \rightarrow CH_4.$$

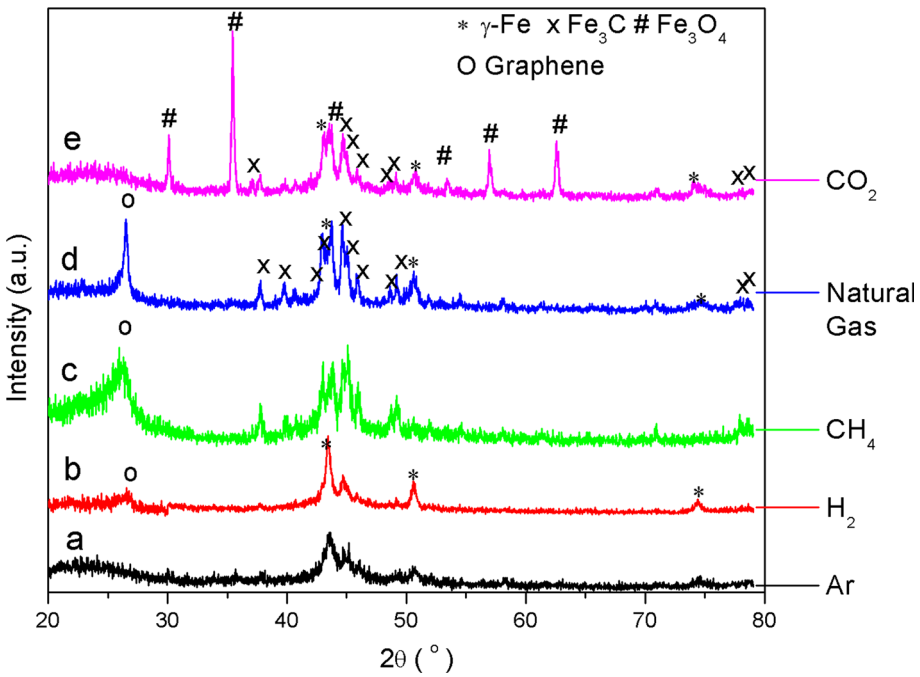

Figure 1 XRD patterns of iron-promoted Kraft lignin sample thermal-treated at 1000°C for 1 h under different atmospheres: **a** argon; **b** hydrogen; **c** methane; **d** natural gas; and **e** carbon dioxide.

There was also a slight peak at 26.55° which corresponds to the graphite (002) plane observed from the sample under hydrogen atmosphere due to methane content increasing along the Fe-lignin sample bed in the reactor. Hydrogen dominates the atmosphere in the inlet of the sample bed, while methane concentration is increasing gradually along the sample bed in the reactor due to the decarburization and hydrogen attacking carbon reactions. There is an equilibrium of C (graphite)-CH_4-H_2 system in the reactor; graphene (or graphite) structures will form over iron particle surface, especially in the outlet of the sample bed.

The XRD pattern of the Fe-lignin sample under methane at 1000°C (Fig. 1c) shows three peaks at 43.50°, 50.64°, and 74.36° that correspond to the γ-iron (111), (2 0 0), and (2 2 0) planes (PDF#98-000-0258). The peaks 37.75°, 40.7°, 42.6°, 43.75°, 44.56°, 44.94°, 45.86°, 49.12°, and 57.8° are assigned to cementite, Fe_3C with correspondence planes of (1 2 1), (2 1 0), (2 0 1), (2 1 1), (1 0 2), (2 2 0), (0 3 1), (1 1 2), and (2 2 1), respectively. There are a few reactions occurring under methane atmosphere:

$$3Fe + CH_4 \rightarrow Fe_3C + 2H_2,$$

$$CH_4 \rightarrow C_{(\gamma-Fe)} + 2H_2.$$

The thermal stability of methane at heat-treating temperatures must be considered. There was a peak at 26.55° which corresponds to the graphite (002) plane observed for the sample of methane atmosphere, and this showed that the graphene structure was formed after the thermal treatment at 1000°C. Similar solid products (Fig. 1d) were obtained under natural gas (NG) atmosphere since methane consists ~ 95% of NG in volume.

Figure 1e shows the XRD pattern of the Fe-lignin sample under CO_2 atmosphere at 1000°C, beside the diffraction peaks to α-Fe, γ-Fe, and Fe3C, where five diffraction peaks at 30.2°, 35.5°, 43.1°, 56.9°, and 62.7° were detected, which corresponded to the diffraction peaks of (2 2 0), (3 1 1), (2 0 8), (5 1 1), and (4 4 0) of Fe_3O_4. This indicated that the solid residue of the Fe-lignin sample under CO_2 atmosphere at 1000°C contained Fe_3O_4 particles. Iron oxides are typical products on the surface of the Fe-lignin sample under CO_2 atmosphere:

$$CO_2 + Fe \rightarrow Fe_3O_4 + CO,$$

$$CO_2 + Fe_3C \rightarrow Fe_3O_4 + CO.$$

TPD-MS results showed that most of the lignin char residue was consumed by the gasification reactions ($Cs + CO_2 = 2CO$) to produce CO under CO_2 atmosphere. The following carburization reactions happened when CO dominated the gas atmosphere,

$$3Fe + 2CO \rightarrow Fe_3C + CO_2,$$

$$2CO \rightarrow C_{(\gamma-Fe)} + CO_2.$$

Based on a calculation by Scherrer equation (see supplement Table 2), the crystallite size of Fe_3O_4 in the sample was 41.6 nm.

Raman spectrum analyses

The Raman spectra can identify the presence of graphite and disordered amorphous carbon in the samples. Figure 2 shows the Raman spectrum of thermal-treated samples of Fe-Kraft lignin under different atmospheres. It was notable that the atmosphere had no influence on the position of peaks in Raman spectra. However, the atmosphere affected the graphitization degree of the samples. The effects of different atmospheres on the degree of graphitization, preferred orientation, and crystalline size of graphite are listed in supplement Table 3. The La value was estimated from the Cançado equation. The values of I_D/I_G decreased with the order of H_2-$< CO_2 < Ar < CH_4 <$ NG, an increase in the uniformity of carbonaceous structure, i.e., as the degree of graphite increased with the order of $H_2 < CO_2 <$ $Ar < CH_4 <$ NG. From Table 3, it can also be found

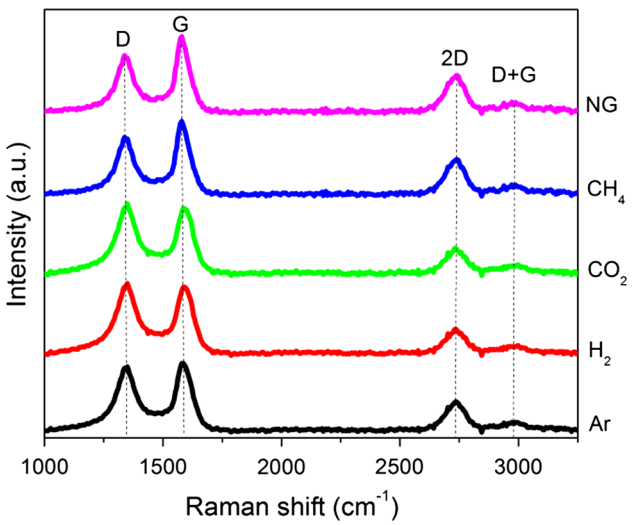

Figure 2 Raman spectra for different purge gases.

that the crystalline size of graphite increases with the order of $H_2 < CO_2 < Ar < CH_4 < NG$.

Morphology

The SEM images of the Fe-lignin sample under argon atmosphere demonstrated a very fine powder structure (Fig. 3a, b). This sample was composed of small particles at low magnification (Fig. 3a). At high magnification, it was observed that the sample was composed of nanoparticles. Spherical-shaped particles with a uniform particle size were observed for the product. These particles had sizes between 5 and 10 nm. XRD results proved these nanoparticles were composed of γ-Fe, iron carbide, and graphene. Figure 3c and d shows SEM images of solid sample produced under a hydrogen flow. It shows porous structures mixed with nanoplates were formed in the solid sample (Fig. 3c). The nanoplates had sizes of 100 nm–1μm with an overall thickness of approximately 1–10 nm (Fig. 3d). XRD results demonstrate these plates are graphene sheets. The morphologies of the Fe-lignin sample produced under CO_2 atmosphere were different than samples from argon and hydrogen (Fig. 3e, f). At low magnification, the surface of the sample treated under CO_2 was smooth and a layer of nanoparticles dispersed homogeneously over the sample surface (Fig. 3e). At high magnification, it was found that the size of nanoparticles ranges from 10 nm to 100 nm (Fig. 3f). XRD results proved these were Fe_3O_4 nanoparticles formed through the oxidation process on the surface of the Fe-lignin sample. The surface morphologies of the solid product under methane are illustrated in Fig. 3g and h. The product had a typically folded and wrinkled sheet structure. XRD results proved these were multilayer graphene nanoplatelets. These graphene nanoplates consisted of several sheets of graphene with an overall thickness of approximately 1–10 nm depending on the controllable process conditions. The product under a natural gas flow showed a similar morphology to that under methane atmosphere (Fig. 3i, j).

Figure 4 displays HRTEM images of the catalytic thermal-treated Fe-Kraft lignin samples under different atmospheres. Small and uniformly distributed iron particles were observed in the sample produced under argon (Fig. 4a–c). HRTEM images of the sample showed the nanoparticles in the sample were core–shell structure with the diameter of the core nanospheres approximately 3–5 nm. The carbon shells exhibiting ordered planes of the graphene structure were observed with 2–10 layers (Fig. 4b). As shown in the HRTEM image (Fig. 4a), Fe@C with uniform particle size was homogenously embedded in the amorphous carbon framework (gray matrix). Figure 4d–f shows bright-field HRTEM images of thermally treated Fe-Kraft lignin sample under H_2. Core–shell nanoparticles were the main products in the sample (Fig. 4d). Nanoiron particles were trapped loosely in graphene shells (Fig. 4e). The lattice space of the dark particle was measured (Fig. 4f), to be 0.208 nm, which corresponds to (111) interlayer space of γ-Fe. HRTEM image also showed the formation of graphene nanosheet in the sample under hydrogen (not shown here). HRTEM images of the sample produced under CO_2 atmosphere are shown in Fig. 4g–i. Sphere- or rectangle-shaped nanoparticles were observed in this sample (Fig. 4g); these particles were usually encapsulated in 1 to 2 layers of graphene (Fig. 4h). Figure 4i shows that Fe_3O_4 composed the top layer of core particle where more than 95% of the particles ranged from 5 to 12 nm. Multilayer graphene nanoplatelets refer to the graphene nanoplates consisting of several sheets (with a range of 2–30 layers) of graphene with an overall thickness of approximately 1–10 nm depending on the controllable process conditions. Figure 4j–l shows the HRTEM images of Fe-lignin sample carbonized at 1000 °C under methane atmosphere. For the Fe-lignin sample carbonized with CH_4, the product contained many graphene sheets as shown in Fig. 4j and k. Figure 4j demonstrates that graphene sheets contain 3–10 layers. As shown in Fig. 4l, the iron carbide was loosely encapsulated by 3–5 layers of graphene shell. HRTEM images (not shown here) of the sample produced under natural gas showed similar results of the sample under methane.

Effect of atmosphere on graphite/graphene production from Fe-lignin samples

Different processing gases were used to investigate the production of graphene materials from Kraft lignin. The solid products were characterized by scanning electron microscopy (SEM), Raman, high-resolution transmission electron microscopy (HRTEM), and X-ray diffraction (XRD); the results are summarized in Table 4. XRD pattern (Fig. 1) shows α-Fe, γ-Fe, and Fe_3C phases observed for the

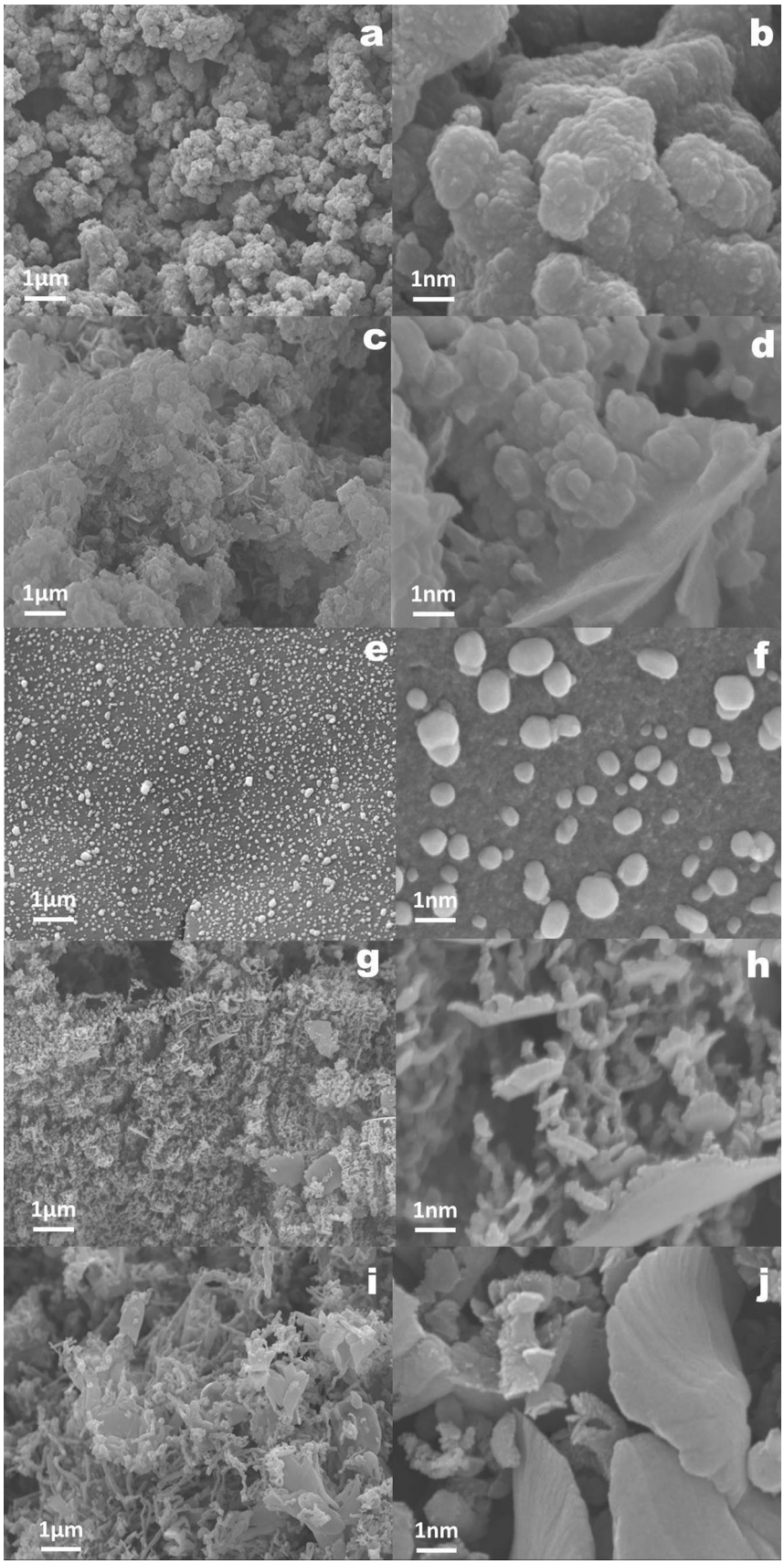

Figure 3 SEM images of iron-promoted Kraft lignin sample thermal-treated at 1000°C under different atmospheres for 1 h: Ar (**a**, **b**), H_2 (**c**, **d**), CO_2 (**e**, **f**), CH_4 (**g**, **h**) and NG (**i**, **j**).

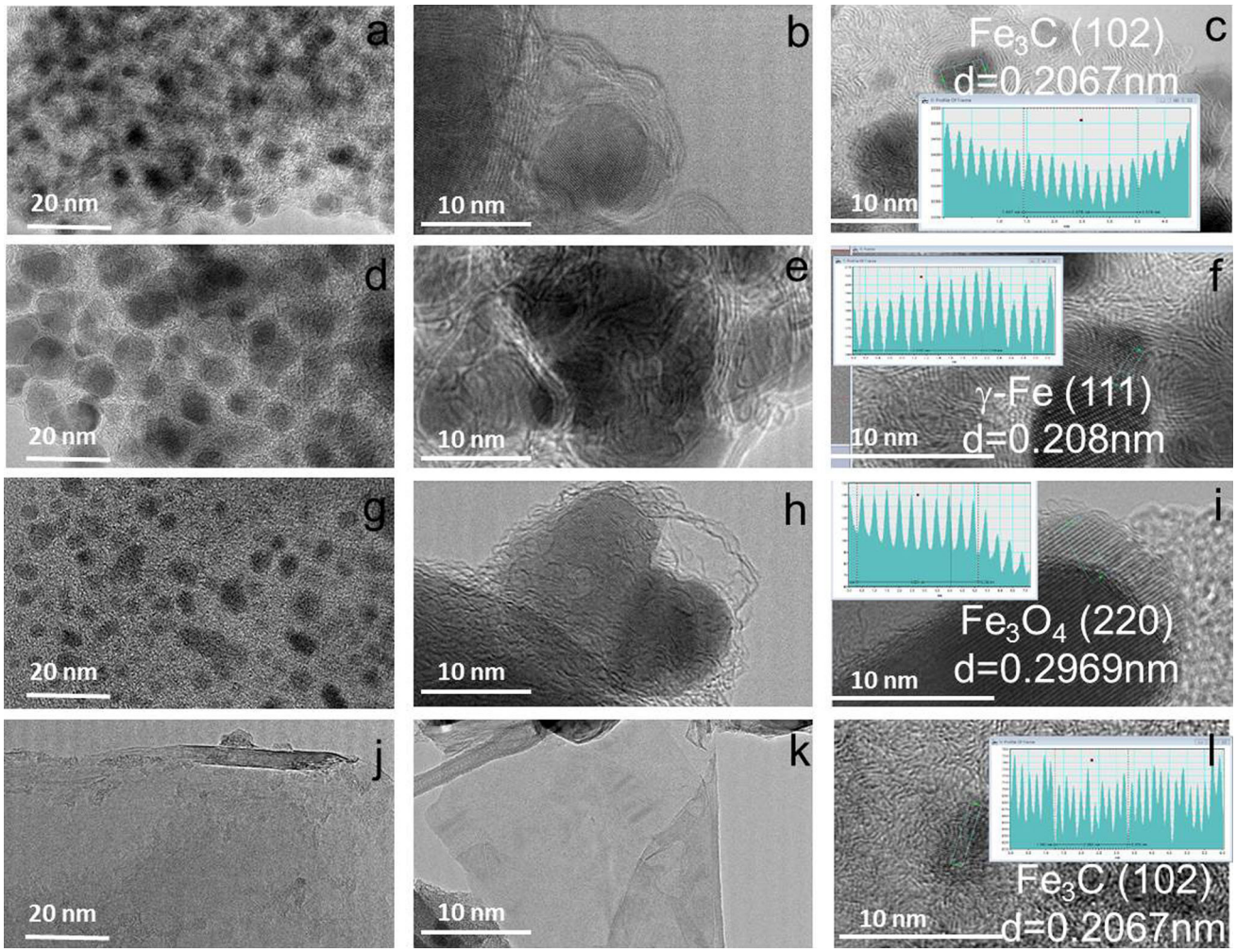

Figure 4 HRTEM images of iron-promoted Kraft lignin sample thermal-treated at 1000°C under different atmospheres for 1 h: Ar (**a**–**c**), H_2 (**d**–**f**), CO_2 (**g**–**i**), and CH_4 (**j**–**l**).

sample under argon; diffraction peaks to α-Fe, γ-Fe, and graphene were detected for the solid sample under hydrogen atmosphere; the diffraction peaks to α-Fe, γ-Fe, Fe_3C, and Fe_3O_4 were found for the sample under CO_2 atmosphere; a significant diffraction peak to graphene was observed for the samples produced under methane and natural gas. Raman results (Fig. 2 and supplement Table 3) demonstrate that the values of I_D/I_G decrease with the order of $H_2 > CO_2 > Ar > CH_4 > NG$ as the degree of graphite increases with the order of $H_2 < CO_2 < Ar < CH_4 < NG$ and the crystalline size of graphene increases with the order of $H_2 < CO_2 < Ar < CH_4 < NG$. SEM images (Fig. 3) show the morphologies of solid samples obtained from Kraft lignin under different atmospheres: 5–10 nm nanoparticles for the sample under argon; 100 nm–1 μm nanosheets with thickness of 1–10 nm for the sample under hydrogen; 10–100 nm Fe3O4 nanoparticles on sample surface for the sample under carbon dioxide; 10 nm–2 μm graphene nanosheets with thickness of 1–3 nm for the sample under methane; and 10 nm–1 μm graphene nanosheets with thickness of 1–10 nm for the sample under NG. HRTEM images (Fig. 4) show the morphologies and microstructures of solid samples obtained from Kraft lignin under different atmospheres: graphene-encapsulated iron particles with 3–5 nm core and 2–10 layers of graphene shell for the sample under argon; iron nanoparticles trapped loosely in graphene shells and graphene nanosheets for the sample under hydrogen; iron nanoparticles encapsulated in 1 to 2 layers of graphene and Fe_3O_4 nanoparticles for the sample under carbon dioxide; graphene nanosheets and graphene-encapsulated iron particles for the

sample under methane; graphene nanosheets and graphene-encapsulated iron particles for the sample under NG.

The experimental results show that the degree of graphitization of Kraft lignin depends not only on the highest temperature, but also on the kind of ambient gas phase during heat treatment. Methane and natural gas in the ambient gas phase seem to accelerate the graphitization, and hydrogen and carbon dioxide have an etching effect on solid carbon species during the catalytic graphitization process, while no noticeable influence is detected with argon.

Conclusion

Multilayer graphene sheets were produced by catalytic graphitization of Kraft lignin under argon, CO_2, methane, NG, and hydrogen atmospheres. The degree of graphitization of Kraft lignin depends not only on the highest temperature, the type of ambient gas phase during heat treatment also has a vital effect on the degree of graphitization of Kraft lignin. Methane and natural gas in the ambient gas phase could accelerate the formation of multilayer graphene materials, and hydrogen and carbon dioxide have an etching effect on solid carbon species during the catalytic graphitization process. The graphene-encapsulated iron particles were the main products under argon; and Fe_3O_4 nanoparticles and graphene-encapsulated iron particles were formed under carbon dioxide.

Acknowledgements

This work was supported by the USDA Forest Service through Grant No. 16-JV-11111124-075. The authors would like to acknowledge Domtar Corp., North Carolina, for providing Kraft lignin for this study. The assistance of Ms. Amanda Lawrence of the Institute for Imaging and Analytical Technologies (I^2AT) at Mississippi State University is gratefully acknowledged.

Electronic supplementary material: The online version of this article (https://doi.org/10.1007/s10853-018-2172-0) contains supplementary material, which is available to authorized users.

References

[1] Ōya A, Marsh H (1982) Phenomena of catalytic graphitization. J Mater Sci 17(2):309–322. https://doi.org/10.1007/BF00591464

[2] Noda Tokiti, Inagaki Michio (1964) Effect of gas phase on graphitization of carbon. Carbon 2:127–130

[3] Noda T, Inagaki M, Sekiya T (1965) Kinetic studies of the graphitization process—I effect of ambient gas phase on the rate of graphitization. Carbon 3:175–180

[4] Yan Q, Toghiani H, Yu F, Cai Z, Zhang J (2011) Effects of pyrolysis conditions on yield of bio-chars from pine chips. For Prod J 61(5):367–371

[5] Okazaki S, Yamaguchi K, Sakamoto A, Ogi T, Okuyama K (2014) Effect of gas atmosphere on graphitization of carbon powder. Kagaku Kogaku Ronbunshu 40(1):12–17

[6] Bachmatiuk A, Boeckl J, Smith H, Ibrahim I, Gemming T, Oswald S, Kazmierczak W, Makarov D, Schmidt OG, Eckert J, Fu LH, Rummeli MH (2015) Vertical graphene growth from amorphous carbon films using oxidizing gases. J Phys Chem C 119(31):17965–17970

[7] Son IH, Park JH, Kwon S, Choi JW, Rümmeli MH (2016) Graphene coating of silicon nanoparticles with CO_2—enhanced chemical vapor deposition. Small 12:658–667. https://doi.org/10.1002/smll.201502880

[8] Hata Kenji, Futaba Don N, Mizuno Kohei, Namai Tatsunori, Yumura Motoo, Iijima Sumio (2004) Water-assisted highly efficient synthesis of impurity-free single-walled carbon nanotubes. Science 306(5700):1362–1364

[9] Vlassiouk I, Regmi M, Fulvio P, Dai S, Datskos P, Eres G, Smirnov S (2011) Role of hydrogen in chemical vapor deposition growth of large single-crystal graphene. ACS Nano 5:6069–6076. https://doi.org/10.1021/nn201978y

[10] Son IH, Song HJ, Kwon S, Bachmatiuk A, Lee SJ, Benayad A, Park JH, Choi J-Y, Chang H, Rümmeli MH (2014) CO_2 enhanced chemical vapor deposition growth of few-layer graphene over NiOx. ACS Nano 8:9224–9232. https://doi.org/10.1021/nn504342e

[11] Mitchel WC, Boeckl J, Tomlin D, Lu W, Rigueur J, Reynolds J (2005) Growth of carbon nanotubes by sublimation of silicon carbide substrates. In: Razeghi M, Brown GJ (eds) International Society for Optics and Photonics, p 77. https://doi.org/10.1117/12.590456

[12] Lu W, Boeckl JJ, Mitchel WC (2010) A critical review of growth of low-dimensional carbon nanostructures on SiC (0 0 0 1): impact of growth environment. J Phys D Appl Phys 43:374004. https://doi.org/10.1088/0022-3727/43/37/374004

[13] Lu WJ, Boeckl J, Mitchel WC, Rigueur J, Collins WE (2006) Role of oxygen in growth of carbon nanotubes on

SiC. Mater Sci Forum 527–529:1575–1578. https://doi.org/10.4028/www.scientific.net/MSF.527-529.1575

[14] Bystrzejewski M, Schönfelder R, Cuniberti G, Lange H, Huczko A, Gemming T, Pichler T, Büchner B, Rümmeli M (2008) Exposing multiple roles of H_2O in high-temperature enhanced carbon nanotube synthesis. Chem Mater 20:6586–6588. https://doi.org/10.1021/cm8020676

[15] Nomura T, Katsura M, Sano T (1973) Graphitization of free carbon precipitating due to the reaction of UC with N2. J Nucl Mater 47:58–64. https://doi.org/10.1016/0022-3115(73)90186-4

[16] Gao L, Ren W, Zhao J, Ma L-P, Chen Z, Cheng H-M (2010) Efficient growth of high-quality graphene films on Cu foils by ambient pressure chemical vapor deposition. Appl Phys Lett 97(18):183109

[17] Losurdo M, Giangregorio MM, Capezzuto P, Bruno G (2011) Graphene CVD growth on copper and nickel: role of hydrogen in kinetics and structure. Phys Chem Chem Phys 13(46):20836–20843

[18] Zhang Y, Li Z, Kim P, Zhang L, Zhou C (2012) Anisotropic hydrogen etching of chemical vapor deposited graphene. ACS Nano 6(1):126–132

[19] Kong J, Cassell AM, Dai H (1998) Chemical vapor deposition of methane for single-walled carbon nanotubes. Chem Phys Lett 292(4–6):567–574

[20] Nikolaev P, Bronikowski MJ, Bradley RK, Rohmund F, Colbert DT, Smith KA, Smalley RE (1999) Gas-phase catalytic growth of single-walled carbon nanotubes from carbon monoxide. Chem Phys Lett 313(1–2):91–97

[21] Xu F, Liu X, Stephen DT (2006) Synthesis of carbon nanotubes on metal alloy substrates with voltage bias in methane inverse diffusion flames. Carbon 44(3):570–577

[22] Sun Z, Yan Z, Yao J, Beitler E, Zhu Y, Tour JM (2010) Growth of graphene from solid carbon sources. Nature 468:549–552. https://doi.org/10.1038/nature09579

[23] Liu X, Fu L, Liu N, Gao T, Zhang Y, Liao L, Liu Z (2011) Segregation growth of graphene on Cu–Ni alloy for precise layer control. J Phys Chem C 115:11976–11982. https://doi.org/10.1021/jp202933u

[24] Zheng M, Takei K, Hsia B, Fang H, Zhang X, Ferralis N, Ko H, Chueh Y-L, Zhang Y, Maboudian R, Javey A (2010) Metal-catalyzed crystallization of amorphous carbon to graphene. Appl Phys Lett 96:63110. https://doi.org/10.1063/1.3318263

[25] Kwak J, Chu JH, Choi J-K, Park S-D, Go H, Kim SY, Park K, Kim S-D, Kim Y-W, Yoon E, Kodambaka S, Kwon S-Y (2012) Near room-temperature synthesis of transfer-free graphene films. Nat. Commun 3:645. https://doi.org/10.1038/ncomms1650

[26] Xie WG, Chen J, Chen J, Ming WW, Deng SZ, Xu NS (2009) Study on effect of hydrogen treatment on amorphous carbon film using scanning probe microscopy. Ultramicroscopy 109(5):451–456

[27] Nasibulin AG, Brown DP, Queipo P, Gonzalez D, Jiang H, Kauppinen EI (2006) An essential role of CO_2 and H_2O during single-walled CNT synthesis from carbon monoxide. Chem Phys Lett 417:179–184

[28] Pimenta MA, Dresselhaus G, Dresselhaus MS, Cançado LG, Jorio A, Saito R (2007) Studying disorder in graphite-based systems by Raman spectroscopy. Phys Chem Chem Phys 9:1276–1290

[29] Abdelaziz Omar Y, Brink Daniel P, Prothmann Jens, Ravi Krithika, Sun Mingzhe, García-Hidalgo Javier, Sandahl Margareta, Hulteberg Christian P, Turner Charlotta, Lidén Gunnar, Gorwa-Grauslun Marie F (2016) Biological valorization of low molecular weight lignin. Biotechnol Adv 34(8):1318–1346

[30] Fengel D, Wegener G (1984) Wood (Chemistry, Ultrastructure, Reactions). Walter de Gruyter, New York